Journal of Materials Chemistry A

ROYAL SOCIETY OF CHEMISTRY

PAPER

View Article Online
View Journal | View Issue

Cite this: J. Mater. Chem. A, 2022, 10, 11238

Tandem organic solar cells with 18.67% efficiency *via* careful subcell design and selection†

Yuzhong Huang,[a] Lingxian Meng,[a] Huazhe Liang,[a] Mingpeng Li,[a] Hongbin Chen,[a] Changzun Jiang,[a] Kai Zhang,[b] Fei Huang,[b] Zhaoyang Yao,[a] Chenxi Li,[a] Xiangjian Wan *[a] and Yongsheng Chen *[a]

Received 28th February 2022
Accepted 21st April 2022

DOI: 10.1039/d2ta01592g

rsc.li/materials-a

The use of tandem structures is an efficient way to simultaneously tackle the absorption and thermalization losses of single junction solar cells and the subcell active layer design and selection always play a crucial role in the construction of tandem organic solar cells. In this work, a wide bandgap acceptor F-ThBr with the fluorene core and brominated thiophene-fused end group has been designed. The device based on D18:F-ThBr offers a PCE of 13.02% with a high V_{oc} of 1.089 V, a J_{sc} of 16.68 mA cm^{-2} and a FF of 71.69%, which makes it a good candidate as a front cell for the construction of tandem OSCs. Meanwhile, in view of the complimentary absorption with F-ThBr and high V_{oc}, PM6:CH1007:$PC_{71}BM$ is selected and optimized as the rear cell. Using the above subcells, a solution-processed tandem OSC is constructed and demonstrates a power conversion efficiency of 18.67%.

1. Introduction

In the past decade, great progress has been made for organic solar cells (OSCs) through intensive efforts on the material design, device optimization and mechanism investigation.[1–9] Currently, power conversion efficiencies (PCEs) over 18% have been achieved for single junction OSCs,[10–18] and the use of ternary and tandem devices has proved to be an effective strategy to further improve the efficiencies of OSCs.[19–22] Despite the great progress in the past few decades, some intrinsic properties of organic materials still limit the efficiencies of OSCs. For example, the thickness of the active layer and thus the device current are limited owing to the generally low charge mobilities and narrow absorption windows of most organic materials. On the other hand, the PCE of a single junction photovoltaic device is confined by the Shockley–Queisser limit,[23] which is independent of the particular type of material. To address these issues, one of the effective strategies is to develop tandem cells with stacking two or more cells with complementary absorption spectra, which can suppress the transmission loss and thermalization losses of single junction solar cells.[24–31] In fact, with the merits of variety and easily tunable bandgaps, organic semiconductor materials are good candidates for fabricating tandem cells. For the widely studied series connected tandem cells, the open circuit voltage (V_{oc}) is the sum of the V_{oc} values of the subcells under ideal conditions. The current density (J_{sc}) is generally limited by the subcell with the smallest one.[27,32] To pursue high efficiency tandem OSCs, many efforts have been devoted to searching for subcells with low energy loss as well as efficient and complimentary sun light absorptions in order to concurrently obtain high V_{oc} and J_{sc} of the tandem cells. In 2018, we had proposed a semi-empirical model which can effectively direct the subcell design and screening. Under the guideline of this semi empirical model, we screened and selected two subcells, *i.e.* PBDB-T:F-M and PCE10:O6T4F:PCBM as the front and rear subcells, respectively, and fabricated a tandem cell with an outstanding PCE of 17.3%.[32] According to the model, high PCE over 25% can be obtained for tandem OSCs if the subcells could have an average energy loss of 0.45 eV, FF over 75% and complimentary absorptions with average EQE above 80%. Despite the realization of the required parameters in single junction devices, there are no active layer materials for subcells which could concurrently meet all the above requirements, especially V_{oc} and J_{sc}, since they are always two entangled parameters for state-of-the-art OSCs. To compromise, the subtle trade off for V_{oc} and J_{sc} has to be considered for the subcell design and screening in order to obtain high efficiency tandem OSCs. Therefore, in our following work, we have proposed and confirmed that high efficiency tandem OSCs could be obtained *via* the subtle trade off of the V_{oc} and J_{sc} of the subcells. Using two subcells with the same polymer donor PBDB-T and two acceptors F-M and NNBDT with complimentary absorptions, an inverted structure tandem cell

[a]*The Centre of Nanoscale Science and Technology, Key Laboratory of Functional Polymer Materials, Institute of Polymer Chemistry, State Key Laboratory of Elemento-Organic Chemistry, College of Chemistry, Renewable Energy Conversion and Storage Center (RECAST), Nankai University, Tianjin 300071, China. E-mail: xjwan@nankai.edu.cn; yschen99@nankai.edu.cn*

[b]*State Key Laboratory of Luminescent Materials and Devices, South China University of Technology, Guangdong, Guangzhou 510640, China*

† Electronic supplementary information (ESI) available. See https://doi.org/10.1039/d2ta01592g

was fabricated and delivered a promising PCE of 14.52%.[33] To date, the above strategy has been effectively used for constructing tandem OSCs and exiting device performances have been achieved.[34] On the other hand, the interconnecting layer (ICL) that links subcells also plays a crucial role in tandem OSCs. All solution processed ICLs should be firstly considered for tandem device fabrication owing to the complexity and high cost of the vacuum evaporation procedure.

With the above analysis and under the guideline of our semi empirical model, herein, we report a tandem OSC with 18.67% efficiency *via* the careful subcell design and screening and using an all solution processed interconnected layer. Firstly, based on non fullerene acceptors with a fluorene core that our group had developed recently, we have designed and synthesized a wide bandgap acceptor F-ThBr with a brominated thiophene-fused end group. The acceptor shows an absorption onset of 730 nm with an E_g of 1.70 eV. The single junction device based on D18:F-ThBr delivered a PCE of 13.03% with a high V_{oc} of 1.089 V, a J_{sc} of 16.68 and a FF of 71.69%. These parameters ensure that D18:F-ThBr is a good candidate as the front cell for tandem OSCs. Secondly, considering the low energy loss and high efficiency of Y6 series single junction OSCs, CH1007 was selected as the rear cell acceptor due to its infrared absorption with the onset around 1000 nm as well as a high V_{oc} value over 0.8 V in a conventional structure single junction device with PM6 as the donor.[35] The inverted structure device based on CH1007 was fabricated and achieved an optimal PCE of 16.56% with a V_{oc} of 0.832 V, J_{sc} of 27.01 mA cm^{-2} and FF of 73.69%. Eventually, using an all solution processed ICL, *i.e.* PEDOT:PSS/ZnO/P4VP, an inverted tandem device was constructed and achieved a high PCE of 18.67% with a V_{oc} of 1.883 V, FF of 70.88% and J_{sc} of 13.99 mA cm^{-2}.

2. Results and discussion

2.1 Front cell design and photovoltaic properties

In the past two decades, for subcell material design, more attention has been focused on rear cell materials with absorptions in the long wavelength range.[26,36–42] However, wide bandgap materials of the front cell always play the same if not a more important role for high efficiency tandem OSC fabrication.[43,44] Besides the requirements of photovoltaic parameters and the absorption range, front cells have to be robust enough to endure the subsequent treatments of the ICL and rear cell. Currently, very few front cells can meet these severe requirements. In the fullerene era, the system P3HT:PCBM had been at a dominant place as a front cell in fabricating tandem OSCs.[29] However, it was limited by its low voltage and moderate current. With the merits of easily tuneable absorptions and energy levels, non fullerene acceptors endow single junction and tandem devices with more opportunities. In our previous work, we have designed an A–D–A acceptor F-M and used it with a polymer donor PBDB-T as a front cell material.[32,45] The front cell delivered a high V_{oc} around 1 V and decent J_{sc} and FF for both inverted and normal structure devices. Based on it and under the guideline of the semi empirical model, an inverted tandem OSC was fabricated and showed an excellent PCE over 17%.[32] For the front cell, despite the fact that F-M is indeed a good acceptor for constructing tandem OSCs, according to the semi empirical model, it is still highly desirable to design acceptor molecules with higher V_{oc} than F-M. With this in mind, herein, we designed an acceptor named F-ThBr *via* introduction a brominated thiophene-fused end group on the same molecular backbone of F-M in view of the relatively weak electron withdrawing ability of the end group and the high V_{oc} of the corresponding IT derivative molecule based device.[46] Thus, an upshifted LUMO and high V_{oc} are expected for its single junction device. As shown in the ESI,† F-ThBr was easily synthesized *via* the Knoevenagel condensation between FDTCHO and the brominated thiophene-fused end group. It has a good solubility in commonly used solvents such chlorobenzene and chloroform.

The UV-vis absorption spectra of F-ThBr are depicted in Fig. 1b. In CF solution, F-ThBr demonstrates the maximum absorption peak at 626 nm. From the solution to solid film, the maximum absorption peak is redshifted about 18 nm, indicating a strong intermolecular interaction in the film. The absorption onset of F-ThBr in the film is around 730 nm, corresponding to an E_g of 1.70 eV. The energy levels of F-ThBr were investigated by cyclic voltammetry. From the onset reduction and oxidation potentials of the CV curves, the LUMO and HOMO levels of F-ThBr were estimated to be −3.69 and −5.70 eV, respectively.

To evaluate the photovoltaic properties of F-ThBr, single junction OSCs with an inverted structure of indium tin oxide (ITO)/ZnO/PFN-Br/D18:F-ThBr/MoO_x/Ag were fabricated. The wide-bandgap polymer D18 was selected as the donor due to its deep HOMO and complementary absorption with F-ThBr (Fig. 1b). For device optimization, we adopted a dual solvent vapor annealing (SVA) strategy, *i.e.* treating the blend film with CB and sequentially with THF SVA. The device optimization details and related photovoltaic parameters are presented in the ESI and summarized in Table S1.† The optimized device delivered a PCE of 13.03% with a high V_{oc} of 1.089 V, a J_{sc} of 16.68 mA cm^{-2} and a FF of 71.69% (Fig. 1d, Table 1). As shown in Fig. 1e, the external quantum efficiency (EQE) curve of the device featured a high photon response covering the range 400 to 700 nm with a maximum value of 82% and over 70% across the range of 500–700 nm. With the absorption onset around 730 nm, and high V_{oc} and EQE values, D18:F-ThBr is expected to be a good candidate as the front cell to construct tandem OSCs.

To understand the good photovoltaic performance of D18:F-ThBr, we characterized the active layer morphology using AFM and GIWAXS (Fig. S3 and S4†). As depicted in Fig. 2a, the optimized active layer of D18:F-ThBr shows a smooth surface morphology with the root-mean-square roughness (R_q) value of 1.08 nm. Compared with the as cast film and the films treated by single solvent vapor annealing, the optimal blend film has a more featured interpenetrating structure, which is favorable for the exciton separation and charge transport. Grazing incidence wide-angle X-ray scattering (GIWAXS) was used to study the molecular stacking of F-ThBr and the blend film. As shown in Fig. S5,† in the neat film, F-ThBr displays a typical face-on orientation with a clear π–π stacking diffraction peak (010) at

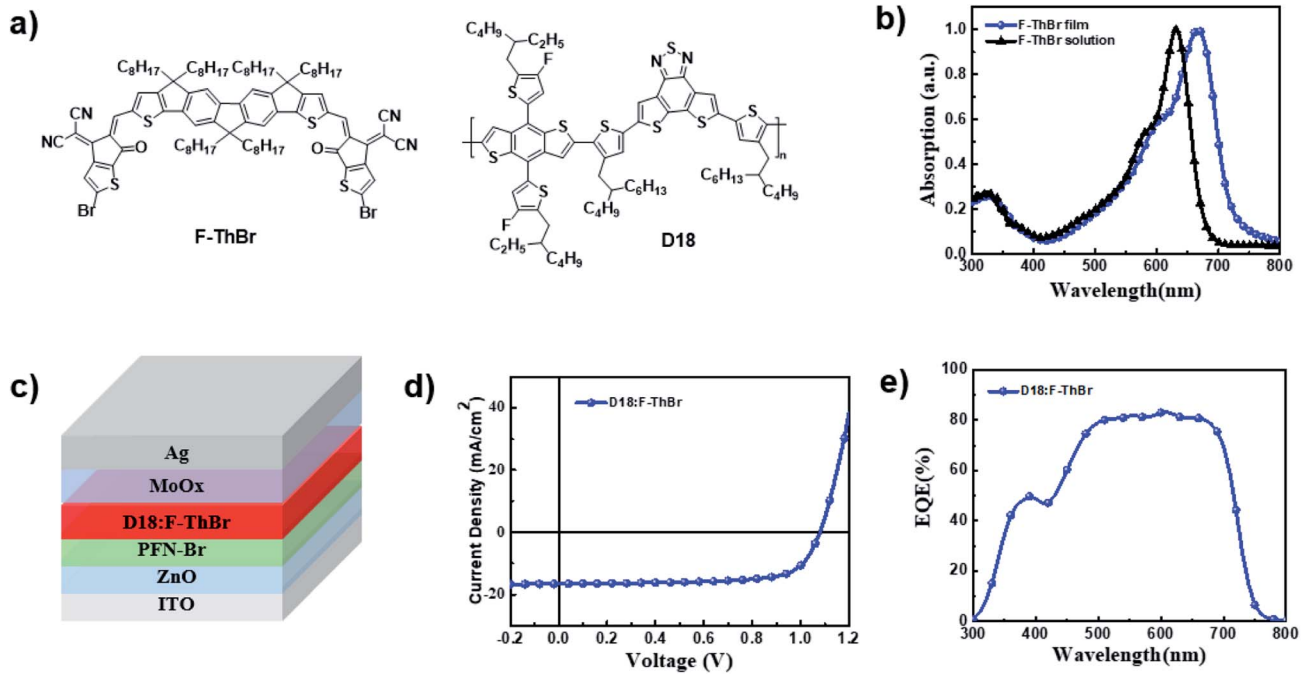

Fig. 1 (a) Chemical structures of F-ThBr and D18. (b) The film and solution absorptions of F-ThBr. (c) Device architecture of D18:F-ThBr. (d) *J*–*V* and (e) EQE curve for the optimized device of D18:F-ThBr.

Table 1 The photovoltaic performance of the single-junction devices based on D18:F-ThBr and PM6:CH1007:$PC_{71}BM$

Active layer	V_{oc} (V)	J_{sc} (mA cm-2)	FF (%)	PCE[a] (%)
D18:F-ThBr	1.089 (1.085 ± 0.002)	16.68 (16.56 ± 0.36)	71.69 (70.01 ± 0.91)	13.03 (12.88 ± 0.12)
PM6:CH1007:$PC_{71}BM$	0.832 (0.835 ± 0.003)	27.01 (26.50 ± 0.40)	73.69 (71.98 ± 1.21)	16.56 (15.95 ± 0.39)

[a] Statistical and optimal results are listed outside of parentheses and in parentheses, respectively, and the average parameters were calculated from 10 independent cells.

1.7 $Å^{-1}$ with a distance of 3.69 Å in the out of plane (OOP) direction. The optimized blend film exhibits a clear lamellar diffraction peak (100) along the IP direction and a π–π stacking diffraction peak (010) in the OOP direction. To further investigate the different microstructures of these films, the crystal coherence length (CCL) values were estimated from the Scherrer equation. The CCL value decreased from 52.3 Å for the as cast film to 43.1 Å for the dual-SVA film. The reduced CCL values indicate that the dual-SVA film is less inclined to aggregate than the as cast film, and results in proper phase separation, which is beneficial for charge transport in the device.

The device of D18:F-ThBr showed a notably high V_{oc} of 1.089 V. To investigate the reason behind it, detailed E_{loss} analysis was conducted. The E_{loss} of the device D18:F-ThBr was calculated to be 0.693 eV following the equation $E_{loss} = E_{gap} - qV_{oc}$, where E_{gap} was estimated by the intersections between the absorption and emission of F-ThBr. Next, the detailed E_{loss} components were investigated based on Shockley–Queisser (SQ) theory.[23] E_{loss} can be divided into three parts: $E_{loss} = \Delta E_1 + \Delta E_2 + \Delta E_3$, where ΔE_1 is the radiative recombination loss above the bandgap, ΔE_2 is the radiative recombination loss below the bandgap, ΔE_3 is the nonradiative energy loss. As summarized in Table S2,† the device showed a ΔE_1 value of 0.284 eV calculated from equation $\Delta E_1 = E_{gap} - qV_{oc}^{SQ}$, comparable with that of other typical OSCs. Calculated from Fourier transform photocurrent spectroscopy (FTPS) and EL spectroscopy, the device gave a V^{rad}_{oc} value of 1.375 V and then we can achieve a ΔE_2 of 0.123 eV following the equation of $\Delta E_2 = qV_{oc}^{SQ} - qV_{oc}^{rad}$. The third part ΔE_3, also named non radiative combination energy loss, was calculated to be 0.270 eV from the EQE of EL (EQE_{EL}) following the equation of $\Delta E_3 = -kT\ln(EQE_{EL})$. Clearly, despite the high V_{oc} of 1.089 V, the overall energy loss of 0.689 eV for D18:F-ThBr is still large mainly due to the big non radiative combination energy loss. Thus, it is still a challenge and meanwhile an opportunity to design front cells with lower energy loss.

2.2 Rear cell screening and photovoltaic properties

As mentioned above, in the past two decades, much effort has been devoted to designing low band gap materials used in rear cells. However, the V_{oc} of a single junction device unavoidably decreases with reducing the bandgap. On the other hand, very few low bandgap systems simultaneously show high V_{oc}, J_{sc} and FF. Therefore, we have proposed that the tradeoff

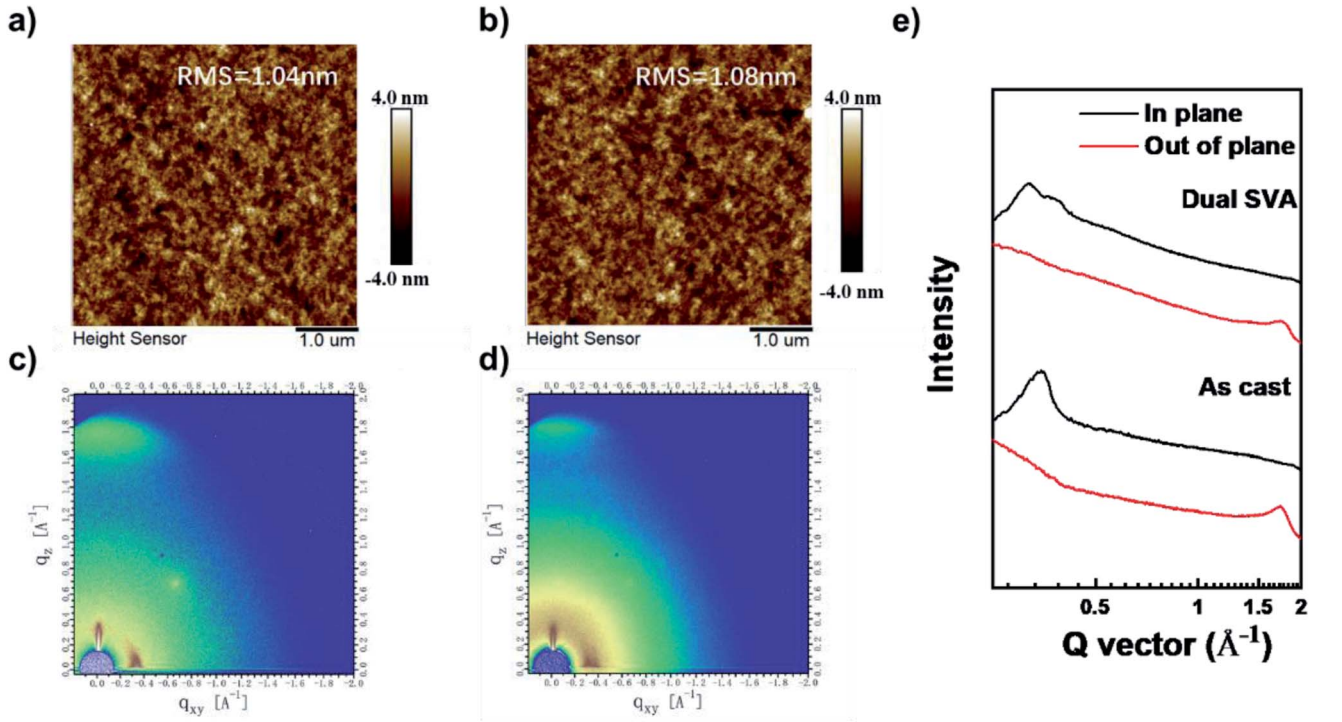

Fig. 2 AFM images for the (a) as cast film of D18:F-ThBr and (b) dual SVA treated film of D18:F-ThBr. GIWAXS pattern for the (c) as cast film of D18:F-ThBr and (d) dual SVA treated film of D18:F-ThBr. (e) In-plane and out-of-plane line cuts of the corresponding GIWAXS patterns.

of V_{oc} and J_{sc} of the subcells is an effective way to achieve high performance tandem OSCs.[33] In state-of-the-art OSCs with a bulk heterojunction structure of the blend film with the donor and acceptor, the acceptor always has a lower band gap than the donor. Thus, when screening the rear cell, we can only consider the absorptions of acceptors of the two subcells, *i.e.* screening the rear cell in which the acceptor has the complimentary absorption with that of the front cell and ignoring the absorption overlapping of donors of the subcells. Meanwhile, the rear cell should have a voltage as high as possible. With this,

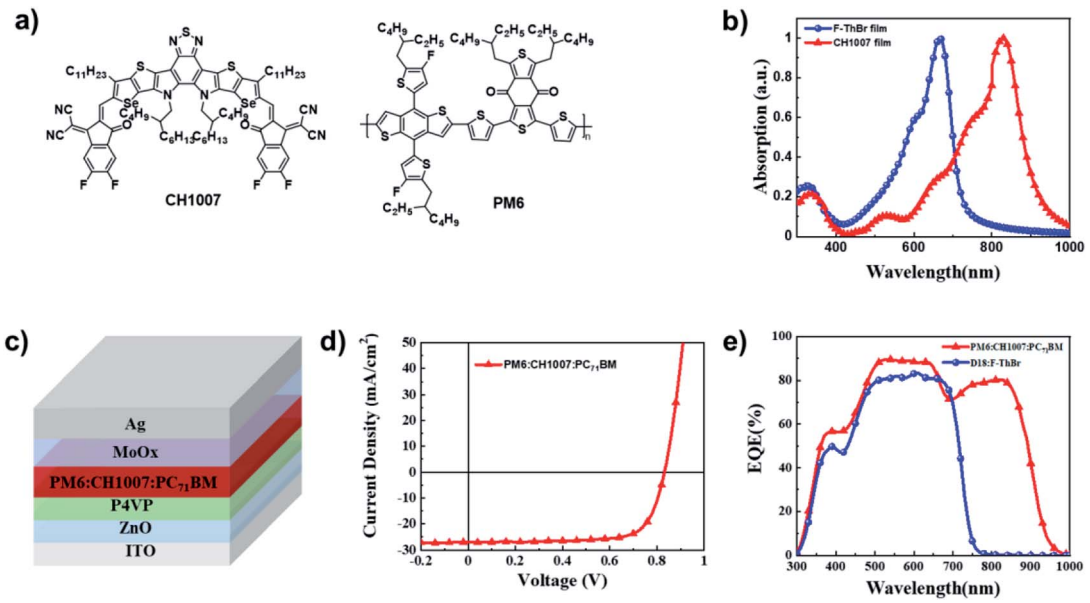

Fig. 3 (a) Chemical structure of acceptors CH1007 and polymer donor PM6. (b) The solid film absorptions of F-ThBr and CH1007. (c) Device architecture of PM6:CH1007:$PC_{71}BM$. (d) *J*–*V* curve of the optimized device of PM6:CH1007:$PC_{71}BM$. (e) EQE curves of the optimized device PM6:CH1007:$PC_{71}BM$ and D18:F-ThBr.

considering the low energy loss and infrared absorption of single junction devices based on Y6 derivatives, CH1007, a Y6 derivative with a near infrared absorption onset around 1000 nm and high V_{oc} over 0.8 V of the corresponding device reported by Alex *et al.*, was screened as the rear cell acceptor (Fig. 3a). As shown in Fig. 3b, CH1007 shows good complimentary absorption with F-ThBr. Despite that the blend film PM6:CH1007:$PC_{71}BM$ in the optimized device demonstrated overlapped absorption with that of D18:F-ThBr in the range 300–700 nm due to the overlapped absorptions of donor polymers D18 and PM6 (Fig. S1†), high efficiency tandem OSCs are still expected with consideration of the tradeoff of V_{oc} and J_{sc} according to the above analysis. Since only normal structure devices were reported for CH1007 and inverted tandem devices will be constructed in this work, we have fabricated and optimized the inverted device of CH1007 with the structure of ITO/ZnO/P4VP/PM6:CH1007:$PC_{71}BM$/MoO_x/Ag (Fig. 3c). It is worth noting that the clearly improved device performance was obtained when poly(4-vinylpyridine) (P4VP) was used as the modified layer on ZnO compared with control devices without a modified layer or with the commonly used PFN-Br (Table S3†). The detailed mechanism is beyond the scope of this work. It was reported that the work function of ZnO was reduced and the active layer morphology of the active layer could be altered owing to the change of the interfacial energy of ZnO after the introduction of P4VP.[47] The details of the device fabrication and performance are provided in the SI. The current density–voltage (J–V) curve of the optimized device is presented in Fig. 3d, which delivered a PCE of 16.56% with a V_{oc} of 0.832 V, J_{sc} of 27.01 mA cm^{-2} and FF of 73.69% (Table 1). The device performance is comparable with that of the reported conventional device. The EQE curves of the optimized device together with that of D18:F-ThBr are shown in Fig. 3e. The device of PM6:CH1007:$PC_{71}BM$ shows a broad and high EQE response in the range 400 and 950 nm. Despite the overlapped EQE for the two single junction devices in the range of 300–700 nm, a much decent J_{sc} can be expected owing to the broad non-overlapped range in 700–950 nm. In addition, the rear cell can also utilize the light in the overlapped range passing through the front cell, which will give the rear cell additional J_{sc}.

2.3 Tandem OSC fabrication and performance

Using the front cell and rear cell as discussed above, we fabricated inverted tandem devices with an all solution process, except for the silver metal electrode. The tandem device architecture and corresponding energy diagram are presented in Fig. 4a and b. A fully solution processed ICL consisting of the modified PEDOT:PSS and ZnO nanoparticle layer modified with P4VP was used. As shown in Fig. 4c, the ICL shows a high transmittance of 95% in the range 400–1100 nm, demonstrating very little absorption loss when used in the tandem device. The detailed optimized parameters are presented in Table S4 in the ESI.† Before the tandem cell optimization, optical simulation modeling using the transfer matrix method was conducted to obtain the possibly optimal thicknesses of the subcells in order to obtain a high and balanced J_{sc} for the tandem device. Fig. 4d displays the simulation results of the dependence of tandem cell J_{sc} *versus* the thicknesses of the front and rear cell active

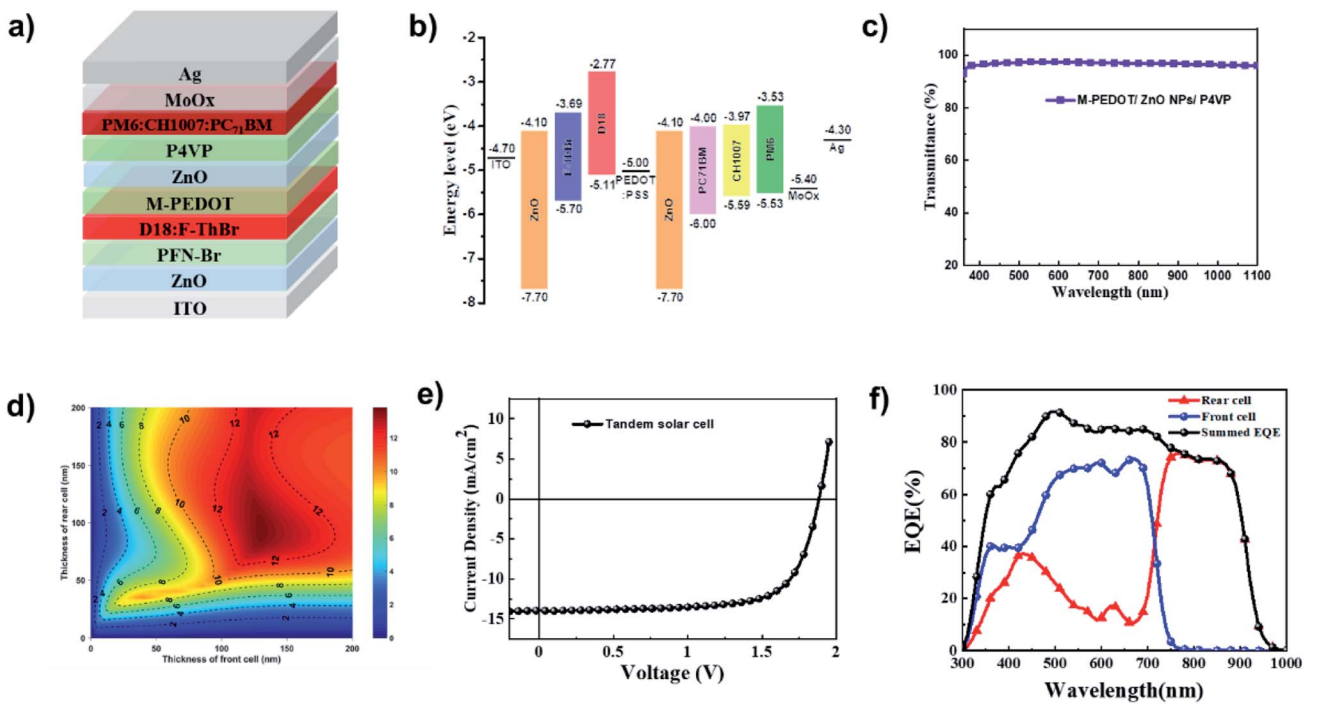

Fig. 4 (a) Device architecture of the tandem cell. (b) Energy level diagram of the tandem cell. (c) Transmission spectrum of the ICL. (d) Simulated current density generated in the tandem cell as a function of the thicknesses of the active layers. (e) J–V curve and (f) EQE curves of the optimized tandem solar cell.

Table 2 Tandem device performance with different thicknesses of the subcells

Thickness (nm)					
Front subcell	Rear subcell	V_{oc} (V)	J_{sc} (mA cm^{-2})	FF (%)	PCE[a] (%)
112 (111.0 ± 3.6)	96 (94.3 ± 4.2)	1.884 (1.881 ± 0.007)	13.34 (12.84 ± 0.36)	71.91 (72.01 ± 1.08)	18.07 (17.41 ± 0.38)
125 (123.2 ± 3.1)	95 (94.1 ± 4.4)	1.883 (1.880 ± 0.011)	13.99 (13.61 ± 0.64)	70.88 (70.85 ± 1.21)	18.67 (18.09 ± 0.48)
140 (141.6 ± 3.1)	97 (94.2 ± 5.1)	1.893 (1.881 ± 0.009)	13.55 (13.25 ± 0.25)	70.70 (70.78 ± 0.50)	18.13 (17.66 ± 0.36)
126 (124.1 ± 3.8)	85 (84.8 ± 3.0)	1.878 (1.881 ± 0.007)	13.49 (12.75 ± 0.34)	70.94 (72.05 ± 1.03)	17.97 (17.29 ± 0.41)
125 (124.5 ± 3.2)	107 (104.5 ± 2.8)	1.875 (1.874 ± 0.009)	13.83 (12.95 ± 0.59)	71.47 (72.49 ± 2.61)	18.53 (17.71 ± 0.66)

[a] Statistical and optimal results are listed outside of parentheses and in parentheses, respectively, and the average parameters were calculated from 10 independent cells.

layers. According to the optical simulation, the best J_{sc} value could be achieved when the thicknesses of the front and rear cell active layers are ~125 and ~100 nm, respectively. Then, the tandem devices were optimized under the direction of the above optical simulation result. The detailed photovoltaic results for difference thicknesses of subcells are summarized in Table 2 and the *J–V* curve of the optimized tandem OSC is shown in Fig. 4e. Finally, the optimal tandem cell demonstrated a PCE of 18.67% with a V_{oc} of 1.883 V, FF of 70.88% and J_{sc} of 13.99 mA cm^{-2}. The V_{oc} of ~1.88 V is approximately equal to the sum of individual V_{oc} of the subcells, indicating that the all solution processed interconnecting layers worked very well in the tandem devices. On the other hand, the annealing treatment of the ICLs can slightly decrease the V_{oc} of the front cell and thus the total V_{oc} of the tandem devices. With the same annealing treatment of ICLs, the V_{oc} of the individual D18:F-ThBr device decreased from 1.089 V to 1.053 V, which is the main reason for the V_{oc} loss of the tandem device.

The EQE of the optimized tandem device is depicted in Fig. 4f. The front cell shows a high photo response in the range of 300–700 nm with the maximum EQE value around 73% at 670 nm. A strong EQE response from ~700 to 900 nm with a maximum value 76% was observed for the rear cell. It is worthy of note that the rear cell also showed a clear EQE response in the overlapped absorption range with the front cell. The J_{sc} values by integration of the EQE curves of the front and rear cells are 13.92 and 13.63 mA cm^{-2}, respectively, which are consistent with J_{sc} in the tandem device from *J–V* measurements.

Besides, the light intensity dependence of the tandem cell performance was measured at different light intensities (Fig. 5). The PCEs of the tandem device remained over 18.4% when the light intensity varied from 6.91 to 99.12 mW cm^{-2}, and a PCE of 18.97% was achieved at a light intensity of 6.91 mW cm^{-2}, which indicates that the tandem device could work efficiently at varied light intensities. In addition, as shown in Fig. 5b, a linear relationship between the light intensity and short-circuit current density was observed, suggesting no substantial space charge build-up in both the two sub-cells and the ICL of the tandem cell. The V_{oc} increases with the light intensity, indicating that the two sub-cells performed well and a good interconnecting layer was achieved.[32,48] Wavelength dependent energy conversion is depicted in Fig. 5c. The total converted energy of the tandem cell is 18.93 mW cm^{-2}, similar to that obtained from the *J–V* curve. Compared to single junction cells, the tandem device has achieved improved performance thanks to the wide range absorptions and efficient EQEs of the two subcells. The initial storage stability of the tandem device and the two single-junction subcell devices were measured. As shown in Fig. S6,† the efficiency of the front cell decreased to 80% of its initial efficiency after 200 h with and without annealing in a glove box with Ar. In contrast, the rear cell and the tandem cell exhibited >97% of the initial efficiency after 200 h without treatment and >90% of the initial efficiency after 200 h under 80 °C. Clearly, even with the relatively unstable front cell, the tandem cell still showed good storage stability thanks to the excellent stability of the rear sub-cell, indicating that the

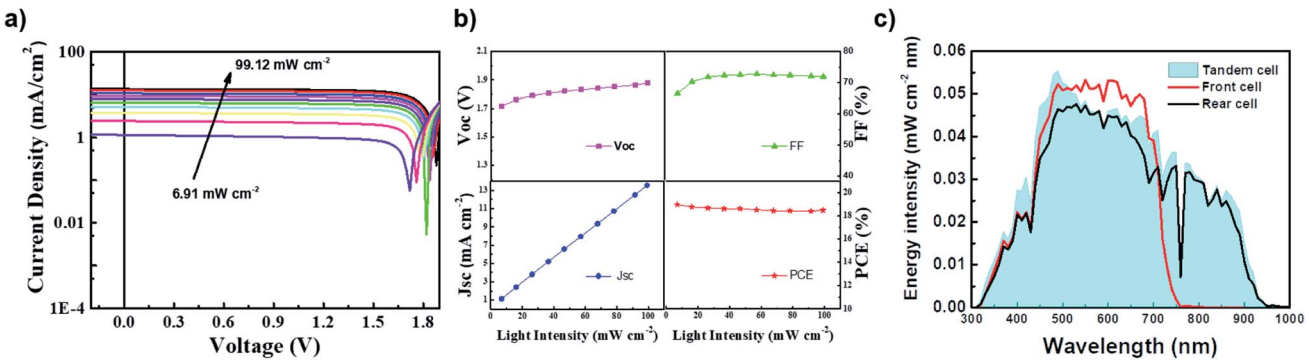

Fig. 5 (a) *J–V* curve and (b) variation of the photovoltaic parameters of the tandem devices at different light intensities from 6.91 to 99.12 mW cm^{-2}. (c) Wavelength-dependent energy density for the subcells and tandem cells (using the method in ref. 24).

tandem device structure might be an alternative strategy to obtain high stability OSCs.[41]

3. Conclusions

In summary, we have fabricated an inverted tandem OSC with an efficiency of 18.67% *via* careful subcell design and selection. Firstly, a wide band gap acceptor F-ThBr was designed and synthesized. A device based on D18:F-ThBr demonstrated a PCE of 13.03% with a high V_{oc} of 1.089 V, J_{sc} of 16.68 mA cm^{-2} and FF of 71.69%. Then the rear cell of PM6:CH007:$PC_{71}BM$ was screened and optimized with a PCE of 16.56% with a V_{oc} of 0.83 V, J_{sc} of 27.01 mA cm^{-2} and FF of 73.69%. Lastly, an inverted tandem cell was fabricated and achieved a high PCE of 18.67% with an all solution processed ICL. This work has highlighted the importance and showcased a good example of the tradeoff of V_{oc} and J_{sc} for subcell design and screening to construct high efficiency tandem cells. It is strongly believed that PCE around 25% can be obtained in near future *via* further delicate subcell material design and screening.

Conflicts of interest

There are no conflicts of interest to declare.

Acknowledgements

The authors thank Yu Chen at the Beijing Synchrotron Radiation Facility, Institute of High Energy Physics for performing GIWAX measurements. The financial support from NSFC (21935007 and 52025033) MoST (2019YFA0705900) of China, Tianjin city (20JCZDJC00740) and 111 Project (B12015) is gratefully acknowledged.

Notes and references

1 A. J. Gillett, A. Privitera, R. Dilmurat, A. Karki, D. Qian, A. Pershin, G. Londi, W. K. Myers, J. Lee, J. Yuan, S.-J. Ko, M. K. Riede, F. Gao, G. C. Bazan, A. Rao, T.-Q. Nguyen, D. Beljonne and R. H. Friend, *Nature*, 2021, **597**, 666.
2 L. Xie, W. Song, J. Ge, B. Tang, X. Zhang, T. Wu and Z. Ge, *Nano Energy*, 2021, **82**, 105770.
3 Y. Wei, J. Yu, L. Qin, H. Chen, X. Wu, Z. Wei, X. Zhang, Z. Xiao, L. Ding, F. Gao and H. Huang, *Energy Environ. Sci.*, 2021, **14**, 2314.
4 Q. He, W. Sheng, M. Zhang, G. Xu, P. Zhu, H. Zhang, Z. Yao, F. Gao, F. Liu, X. Liao and Y. Chen, *Adv. Energy Mater.*, 2021, **11**, 2003390.
5 L. Ye, K. Weng, J. Xu, X. Du, S. Chandrabose, K. Chen, J. Zhou, G. Han, S. Tan, Z. Xie, Y. Yi, N. Li, F. Liu, J. M. Hodgkiss, C. J. Brabec and Y. Sun, *Nat. Commun.*, 2020, **11**, 6005.
6 Q. Liu, Y. Jiang, K. Jin, J. Qin, J. Xu, W. Li, J. Xiong, J. Liu, Z. Xiao, K. Sun, S. Yang, X. Zhang and L. Ding, *Sci. Bull.*, 2020, **65**, 272.
7 X. Ke, L. Meng, X. Wan, M. Li, Y. Sun, Z. Guo, S. Wu, H. Zhang, C. Li and Y. Chen, *J. Mater. Chem. A*, 2020, **8**, 9726.
8 X. Du, T. Heumueller, W. Gruber, O. Almora, A. Classen, J. Qu, F. He, T. Unruh, N. Li and C. J. Brabec, *Adv. Mater.*, 2020, **32**, 1908305.
9 J. Yuan, Y. Zhang, L. Zhou, G. Zhang, H.-L. Yip, T.-K. Lau, X. Lu, C. Zhu, H. Peng, P. A. Johnson, M. Leclerc, Y. Cao, J. Ulanski, Y. Li and Y. Zou, *Joule*, 2019, **3**, 1140.
10 J. Zhang, F. Bai, I. Angunawela, X. Xu, S. Luo, C. Li, G. Chai, H. Yu, Y. Chen, H. Hu, Z. Ma, H. Ade and H. Yan, *Adv. Energy Mater.*, 2021, **11**, 2102596.
11 H. Meng, C. Liao, M. Deng, X. Xu, L. Yu and Q. Peng, *Angew. Chem., Int. Ed.*, 2021, **60**, 22554.
12 L. Liu, S. Chen, Y. Qu, X. Gao, L. Han, Z. Lin, L. Yang, W. Wang, N. Zheng, Y. Liang, Y. Tan, H. Xia and F. He, *Adv. Mater.*, 2021, **33**, 2101279.
13 F. Liu, L. Zhou, W. Liu, Z. Zhou, Q. Yue, W. Zheng, R. Sun, W. Liu, S. Xu, H. Fan, L. Feng, Y. Yi, W. Zhang and X. Zhu, *Adv. Mater.*, 2021, **33**, 2100830.
14 C. Li, J. Zhou, J. Song, J. Xu, H. Zhang, X. Zhang, J. Guo, L. Zhu, D. Wei, G. Han, J. Min, Y. Zhang, Z. Xie, Y. Yi, H. Yan, F. Gao, F. Liu and Y. Sun, *Nat. Energy*, 2021, **6**, 605.
15 L. Hong, H. Yao, Y. Cui, P. Bi, T. Zhang, Y. Cheng, Y. Zu, J. Qin, R. Yu, Z. Ge and J. Hou, *Adv. Mater.*, 2021, **33**, 2103091.
16 C. Guo, D. Li, L. Wang, B. Du, Z.-X. Liu, Z. Shen, P. Wang, X. Zhang, J. Cai, S. Cheng, C. Yu, H. Wang, D. Liu, C.-Z. Li and T. Wang, *Adv. Energy Mater.*, 2021, **11**, 2102000.
17 Y. Cui, Y. Xu, H. Yao, P. Bi, L. Hong, J. Zhang, Y. Zu, T. Zhang, J. Qin, J. Ren, Z. Chen, C. He, X. Hao, Z. Wei and J. Hou, *Adv. Mater.*, 2021, **33**, 2102420.
18 Y. Lin, M. I. Nugraha, Y. Firdaus, A. D. Scaccabarozzi, F. Aniés, A.-H. Emwas, E. Yengel, X. Zheng, J. Liu, W. Wahyudi, E. Yarali, H. Faber, O. M. Bakr, L. Tsetseris, M. Heeney and T. D. Anthopoulos, *ACS Energy Lett.*, 2020, **5**, 3663.
19 X. Ma, A. Zeng, J. Gao, Z. Hu, C. Xu, J. H. Son, S. Y. Jeong, C. Zhang, M. Li, K. Wang, H. Yan, Z. Ma, Y. Wang, H. Y. Woo and F. Zhang, *Natl. Sci. Rev.*, 2021, **8**, nwaa305.
20 C. Xu, Z. Zhao, K. Yang, L. Niu, X. Ma, Z. Zhou, X. Zhang and F. Zhang, *J. Mater. Chem. A*, 2022, **10**, 6291.
21 W. Xu, X. Ma, J. H. Son, S. Y. Jeong, L. Niu, C. Xu, S. Zhang, Z. Zhou, J. Gao, H. Y. Woo, J. Zhang, J. Wang and F. Zhang, *Small*, 2022, **18**, 2104215.
22 T. Ameri, G. Dennler, C. Lungenschmied and C. J. Brabec, *Energy Environ. Sci.*, 2009, **2**, 347.
23 W. Shockley and H. J. Queisser, *J. Appl. Phys.*, 1961, **32**, 510.
24 L. Zuo, X. Shi, S. B. Jo, Y. Liu, F. Lin and A. K. Y. Jen, *Adv. Mater.*, 2018, **30**, 1706816.
25 S. Lu, X. Guan, X. Li, W. E. I. Sha, F. Xie, H. Liu, J. Wang, F. Huang and W. C. H. Choy, *Adv. Energy Mater.*, 2015, **5**, 1500631.
26 T. Ameri, N. Li and C. J. Brabec, *Energy Environ. Sci.*, 2013, **6**, 2390.
27 O. Adebanjo, P. P. Maharjan, P. Adhikary, M. Wang, S. Yang and Q. Qiao, *Energy Environ. Sci.*, 2013, **6**, 3150.
28 L. Yang, H. Zhou, S. C. Price and W. You, *J. Am. Chem. Soc.*, 2012, **134**, 5432.

29 S. Sista, Z. Hong, L.-M. Chen and Y. Yang, *Energy Environ. Sci.*, 2011, **4**, 1606.
30 A. Hadipour, B. de Boer and P. W. M. Blom, *Adv. Funct. Mater.*, 2008, **18**, 169.
31 G. Dennler, M. C. Scharber, T. Ameri, P. Denk, K. Forberich, C. Waldauf and C. J. Brabec, *Adv. Mater.*, 2008, **20**, 579.
32 L. Meng, Y. Zhang, X. Wan, C. Li, X. Zhang, Y. Wang, X. Ke, Z. Xiao, L. Ding, R. Xia, H.-L. Yip, Y. Cao and Y. Chen, *Science*, 2018, **361**, 1094.
33 L. Meng, Y.-Q.-Q. Yi, X. Wan, Y. Zhang, X. Ke, B. Kan, Y. Wang, R. Xia, H.-L. Yip, C. Li and Y. Chen, *Adv. Mater.*, 2019, **31**, 1804723.
34 Z. Zheng, J. Wang, P. Bi, J. Ren, Y. Wang, Y. Yang, X. Liu, S. Zhang and J. Hou, *Joule*, 2022, **6**, 171.
35 F. Lin, K. Jiang, W. Kaminsky, Z. Zhu and A. K. Y. Jen, *J. Am. Chem. Soc.*, 2020, **142**, 15246.
36 W. Li, A. Furlan, K. H. Hendriks, M. M. Wienk and R. A. Janssen, *J. Am. Chem. Soc.*, 2013, **135**, 5529.
37 P. Cheng and Y. Yang, *Acc. Chem. Res.*, 2020, **53**, 1218.
38 K. Gao, Y. Kan, X. Chen, F. Liu, B. Kan, L. Nian, X. Wan, Y. Chen, X. Peng, T. P. Russell, Y. Cao and A. K. Y. Jen, *Adv. Mater.*, 2020, **32**, 1906129.
39 K. H. Hendriks, W. Li, M. M. Wienk and R. A. J. Janssen, *J. Am. Chem. Soc.*, 2014, **136**, 12130.
40 Z. Xiao, X. Jia, D. Li, S. Wang, X. Geng, F. Liu, J. Chen, S. Yang, T. P. Russell and L. Ding, *Sci. Bull.*, 2017, **62**, 1494.
41 Z. Jia, S. Qin, L. Meng, Q. Ma, I. Angunawela, J. Zhang, X. Li, Y. He, W. Lai, N. Li, H. Ade, C. J. Brabec and Y. Li, *Nat. Commun.*, 2021, **12**, 178.
42 H. Yao, Y. Cui, R. Yu, B. Gao, H. Zhang and J. Hou, *Angew. Chem., Int. Ed.*, 2017, **56**, 3045.
43 Y. Cui, Y. Wang, J. Bergqvist, H. Yao, Y. Xu, B. Gao, C. Yang, S. Zhang, O. Inganäs, F. Gao and J. Hou, *Nat. Energy*, 2019, **4**, 768.
44 G. Liu, J. Jia, K. Zhang, X. e. Jia, Q. Yin, W. Zhong, L. Li, F. Huang and Y. Cao, *Adv. Energy Mater.*, 2019, **9**, 1803657.
45 H.-H. Gao, Y. Sun, Y. Cai, X. Wan, L. Meng, X. Ke, S. Li, Y. Zhang, R. Xia, N. Zheng, Z. Xie, C. Li, M. Zhang, H.-L. Yip, Y. Cao and Y. Chen, *Adv. Energy Mater.*, 2019, **9**, 1901024.
46 Z. Luo, T. Liu, Y. Xiao, T. Yang, Z. Chen, G. Zhang, C. Zhong, R. Ma, Y. Chen, Y. Zou, X. Lu, H. Yan and C. Yang, *Nano Energy*, 2019, **66**, 104146.
47 A. Sharma, R. Kroon, D. A. Lewis, G. G. Andersson and M. R. Andersson, *ACS Appl. Mater. Interfaces*, 2017, **9**, 10929.
48 J. You, L. Dou, K. Yoshimura, T. Kato, K. Ohya, T. Moriarty, K. Emery, C.-C. Chen, J. Gao, G. Li and Y. Yang, *Nat. Commun.*, 2013, **4**, 1446.